


# Loss of autophagy protein ATG5 impairs cardiac capacity in mice and humans through diminishing mitochondrial abundance and disrupting Ca<sup>2+</sup> cycling

Senka Ljubojević-Holzer<sup>1,2†</sup>, Simon Kraler <sup>1†</sup>, Nataša Djalinač<sup>1</sup>, Mahmoud Abdellatif <sup>1</sup>, Julia Voglhuber <sup>1,2</sup>, Julia Schipke <sup>3</sup>, Marlene Schmidt <sup>4</sup>, Katharina-Maria Kling<sup>3</sup>, Greta Therese Franke<sup>3</sup>, Viktoria Herbst<sup>1</sup>, Andreas Zirlik <sup>1</sup>, Dirk von Lewinski <sup>1</sup>, Daniel Scherr<sup>1</sup>, Peter P. Rainer <sup>1</sup>, Michael Kohlhaas <sup>4</sup>, Alexander Nickel<sup>4</sup>, Christian Mühlfeld<sup>3</sup>, Christoph Maack <sup>4</sup>, and Simon Sedej <sup>1,2,5\*</sup>

<sup>1</sup>Department of Cardiology, Medical University of Graz, Auenbruggerplatz 15, 8036 Graz, Austria; <sup>2</sup>BioTechMed Graz, Mozartgasse 12/II, 8010 Graz, Austria; <sup>3</sup>Institute of Functional and Applied Anatomy, Hannover Medical School, Carl-Neuberg-Str. 1, 30625 Hannover, Germany; <sup>4</sup>Department of Translational Research, Comprehensive Heart Failure Center (CHFC), University Clinic Würzburg, Am Schwarzenberg 15, Haus A15, 97078 Würzburg, Germany; and <sup>5</sup>Institute of Physiology, Faculty of Medicine, University of Maribor, 2000 Maribor, Slovenia

Received 23 January 2021; editorial decision 17 March 2021; accepted 19 March 2021; online publish-ahead-of-print 22 March 2021

**Time for primary review: 15 days**

## Aims

Autophagy protects against the development of cardiac hypertrophy and failure. While aberrant Ca<sup>2+</sup> handling promotes myocardial remodelling and contributes to contractile dysfunction, the role of autophagy in maintaining Ca<sup>2+</sup> homeostasis remains elusive. Here, we examined whether *Atg5* deficiency-mediated autophagy promotes early changes in subcellular Ca<sup>2+</sup> handling in ventricular cardiomyocytes, and whether those alterations associate with compromised cardiac reserve capacity, which commonly precedes the onset of heart failure.

## Methods and results

RT-qPCR and immunoblotting demonstrated reduced *Atg5* gene and protein expression and decreased abundance of autophagy markers in hypertrophied and failing human hearts. The function of ATG5 was examined using cardiomyocyte-specific *Atg5*-knockout mice (*Atg5*<sup>-/-</sup>). Before manifesting cardiac dysfunction, *Atg5*<sup>-/-</sup> mice showed compromised cardiac reserve in response to β-adrenergic stimulation. Consequently, effort intolerance and maximal oxygen consumption were reduced during treadmill-based exercise tolerance testing. Mechanistically, cellular imaging revealed that *Atg5* deprivation did not alter spatial and functional organization of intracellular Ca<sup>2+</sup> stores or affect Ca<sup>2+</sup> cycling in response to slow pacing or upon acute isoprenaline administration. However, high-frequency stimulation exposed stunted amplitude of Ca<sup>2+</sup> transients, augmented nucleoplasmic Ca<sup>2+</sup> load, and increased CaMKII activity, especially in the nuclear region of hypertrophied *Atg5*<sup>-/-</sup> cardiomyocytes. These changes in Ca<sup>2+</sup> cycling were recapitulated in hypertrophied human cardiomyocytes. Finally, ultrastructural analysis revealed accumulation of mitochondria with reduced volume and size distribution, meanwhile functional measurements showed impaired redox balance in *Atg5*<sup>-/-</sup> cardiomyocytes, implying energetic unsustainability due to overcompensation of single mitochondria, particularly under increased workload.

## Conclusion

Loss of cardiac *Atg5*-dependent autophagy reduces mitochondrial abundance and causes subtle alterations in subcellular Ca<sup>2+</sup> cycling upon increased workload in mice. Autophagy-related impairment of Ca<sup>2+</sup> handling is progressively worsened by β-adrenergic signalling in ventricular cardiomyocytes, thereby leading to energetic exhaustion and compromised cardiac reserve.

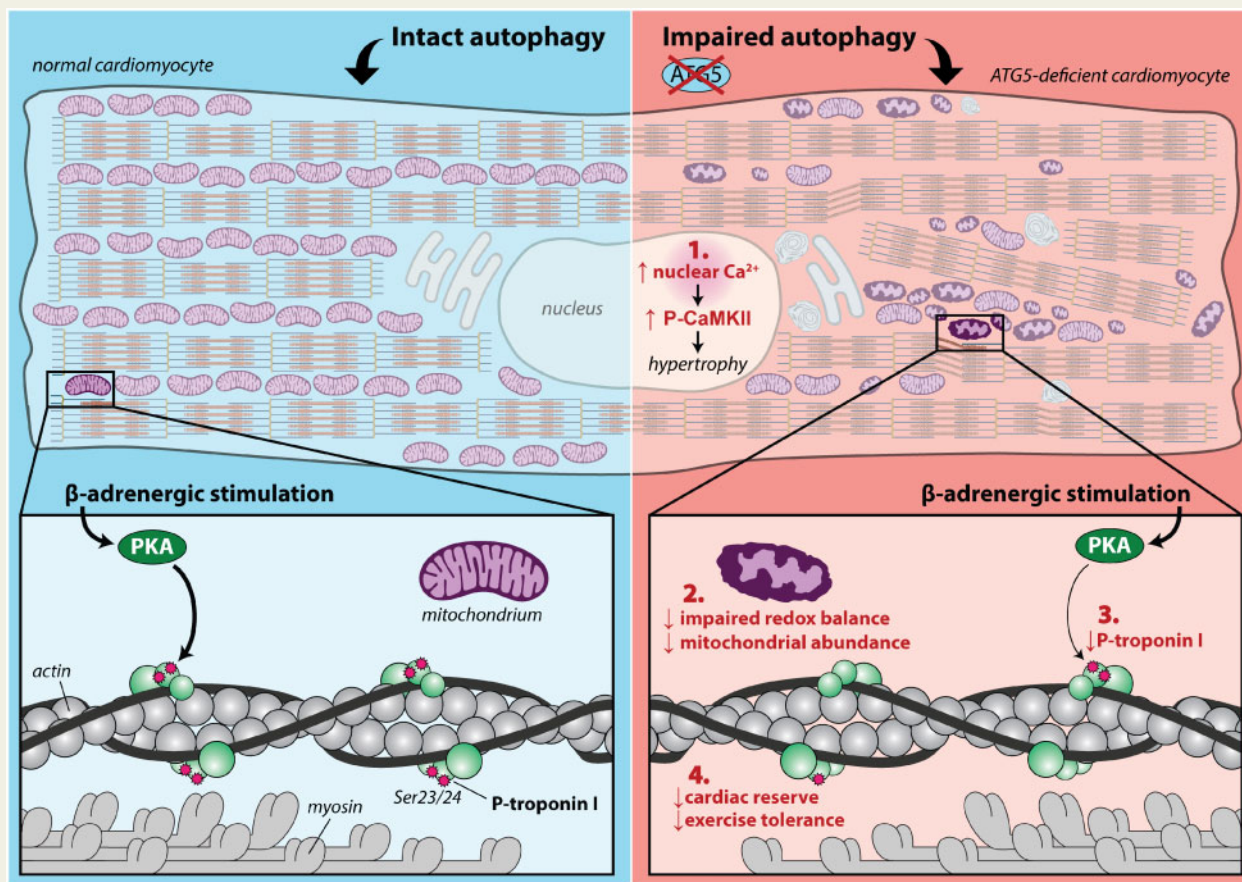
\* Corresponding author. Tel: +43 316 385 72742, E-mail: simon.sedej@medunigraz.at

†The first two authors contributed equally to the study.

© The Author(s) 2021. Published by Oxford University Press on behalf of the European Society of Cardiology.

This is an Open Access article distributed under the terms of the Creative Commons Attribution Non-Commercial License (<http://creativecommons.org/licenses/by-nc/4.0/>), which permits non-commercial re-use, distribution, and reproduction in any medium, provided the original work is properly cited. For commercial re-use, please contact [journals.permissions@oup.com](mailto:journals.permissions@oup.com)

## Graphical Abstract



## Keywords

Cardiomyocytes • Calcium • Mitochondria • Autophagy • Beta-adrenergic signalling

## 1. Introduction

Macroautophagy (hereafter referred to as autophagy) is a key protective process necessary for cardiac homeostasis.<sup>1,2</sup> Under physiological conditions, constitutive autophagy maintains structure and function of the heart by eliminating damaged molecules and dysfunctional organelles from the cytoplasm, which might otherwise elicit harmful effects to cardiac cells, including long-lived cardiomyocytes.<sup>1,3,4</sup> Autophagy-related proteins (ATG) are essential in this process, among which ATG5 is indispensable for the early phase of autophagosome formation. Mice with cardiomyocyte-restricted *Atg5* deletion display increased ubiquitination, mitochondrial aggregates and disorganized sarcomere structure in cardiomyocytes.<sup>5</sup> Despite early structural deteriorations within *Atg5* null cardiomyocytes, cardiac function is remarkably normal until early adulthood. Hence, it has been argued that a mechanism, such as the *Atg5/Atg7*-independent alternative autophagy<sup>6</sup> and/or chaperone-mediated autophagy<sup>7</sup> may compensate for *Atg5* deficiency to limit cardiac damage. However, such cardioprotective mechanism efficiently operates against adverse remodelling only temporarily, because cardiomyocyte-specific *Atg5*-deficient mice develop left

ventricular hypertrophy that shortly thereafter progresses to heart failure, resulting ultimately in premature death.<sup>5</sup>

Mechanistically, long-term absence of basal autophagy is associated with reduced mitochondrial respiratory function and increased oxidative stress, which predisposes exhausted cardiomyocytes to apoptotic cell death and contractility decline. In addition, the absence of essential autophagy-related proteins may also cause perturbations of other inter-related cellular mechanisms,<sup>8</sup> which in conjunction with damaged mitochondria initiate and drive adverse remodelling and contractile dysfunction. Notably, disturbed Ca<sup>2+</sup> handling is one such early abnormality during adverse myocardial remodelling<sup>9</sup> that causes heart failure.<sup>10,11</sup> In this regard, autophagy-deprived hearts exhibit compromised energy and redox balance due to increased number of ill-functioning mitochondria. Such perturbations may cause shifts in ionic gradients and attenuate excitability by deregulating the energy-demanding process of intracellular Ca<sup>2+</sup> homeostasis, especially under increased workload. Besides cytoplasmic and mitochondrial Ca<sup>2+</sup> changes, altered nucleoplasmic Ca<sup>2+</sup> signalling could be critical to functional remodelling of cardiomyocytes, which lack autophagy, as activation of nuclear Ca<sup>2+</sup>-mediated hypertrophic gene program affects protein expression, including components of

the excitation–contraction coupling machinery.<sup>9</sup> To this end, however, it remains unknown whether absence of cardiac autophagy alters subcellular  $\text{Ca}^{2+}$  cycling at early stages of remodelling that precede the development of heart failure.

In this study, we examined the ATG5 expression at the transcriptional and protein levels in non-failing, hypertrophic and failing human hearts. We then used cardiomyocyte-specific *Atg5*-deficient mice before they develop heart failure to identify the specific role of ATG5 in subcellular  $\text{Ca}^{2+}$  cycling under normal and stressed conditions. Finally, we functionally assessed the translational potential of our findings in hypertrophied human cardiomyocytes.

## 2. Methods

A detailed description of methods is available in [Supplementary material online](#).

### 2.1 Ethics

Animal experiments were performed in accordance with European ethical regulation (Directive 2010/63/EU) and approved by the responsible Austrian government agency (BMBWF: 66.010/0038-WFN/3b/2017; BMBWF-66.010/0208-V/3b/2018). Procedures involving human samples were approved by the Ethical Committee of the Medical University of Graz (28-508 ex 15/16), and performed in accordance with principles outlined in the *Declaration of Helsinki*. Informed written consent was not feasible to obtain because the patients were not able to give the informed consent as a result of their underlying medical condition. The requirement for informed consent was waived by the ethical committee. Patients' characteristics are described in [Supplementary material online, Table S1](#). Donor hearts were explanted post-mortem together with other organs. Upon ice-cold cardioplegia, cardiac biopsies were harvested from the left ventricular free wall, quickly frozen in liquid nitrogen and stored at  $-80^{\circ}\text{C}$  for future analysis.

### 2.2 Mice

Cardiomyocyte-specific *Atg5* knock-out mice (*Atg5*<sup>-/-</sup> mice;  $N = 52$ ) were generated from *Atg5*<sup>flox/flox</sup> mice crossed with heterozygous knock-in mice that express Cre<sup>+</sup> recombinase driven by the cardiomyocyte-specific  $\alpha$ -myosin light chain (MLC2a-Cre) gene promoter.<sup>12</sup> We used *Atg5*<sup>-/-</sup> male mice between 12 and 15 weeks, because at this age they present a normal cardiac phenotype despite a complete block of autophagy.<sup>4,5</sup> Age-matched *Atg5*<sup>+/+</sup> male littermates served as controls ( $N = 45$ ).

### 2.3 Haemodynamic measurements and cardiac stress testing

Haemodynamic assessment was performed according to the established protocol.<sup>4</sup> Mice were sedated with isoflurane (5% for induction and 1–2% for maintenance), intubated, and mechanically ventilated (Harvard Mini-Vent, type 845, Harvard Apparatus). A pressure-conductance catheter (SPR-839; Millar Instruments) was inserted into the right carotid artery and advanced into the LV, where pressure signals were recorded (MPVS ultra, Millar Instruments), and analysed offline (LabChart 8 Pro, AD Instruments). Cardiac parameters were measured at baseline and after intraperitoneal isoprenaline administration ( $2\ \mu\text{g}/\text{kg}$  body weight<sup>13</sup>) to evaluate cardiac reserve capacity. After assessment of haemodynamic parameters that were averaged from 10 consecutive beats with ventilation suspended at end-expiration, mice were euthanized by decapitation.

Hearts were rapidly frozen in liquid nitrogen and stored at  $-80^{\circ}\text{C}$  for molecular analysis.

### 2.4 Treadmill running coupled to indirect calorimetry

A subset of mice ( $N = 16$ ) underwent peak effort testing on a motorized treadmill coupled to a calorimetric unit (TSE Systems, Germany). Mice were subjected to a ramp exercise protocol with an initial velocity of 3 m/min followed by a constant acceleration of 3 m/min<sup>2</sup> at 0° inclination.<sup>14</sup> The exercise ended at the maximal exhaustion, which was defined as the mouse's inability to maintain running speed despite being in contact with the electrical grid for five consecutive seconds. Maximal oxygen consumption ( $\text{VO}_2\text{max}$ ) and run distance were determined at the point at which oxygen uptake reached a plateau during exhaustive workout/exercise.

### 2.5 Real-time quantitative PCR (RT–qPCR)

Total purification of mouse and human RNA and measurements of RNA yield and quality were performed as described previously.<sup>15</sup> cDNA was synthesized using the QuantiTect Reverse Transcription kit (for mouse; Qiagen, Hilden, Germany) and the HighCapacity cDNA RT Kit (for human; Thermo Fisher Scientific, Wilmington, USA), respectively. RT–qPCR was performed with cDNA at a concentration of 10 ng per 10  $\mu\text{L}$  reaction volume. TaqMan Gene Expression Assays were used for all qPCR experiments following the protocol outlined in [Supplementary material online, Tables S2 and S3](#). Primer efficiency correction was performed with GenEx 5.4.4. Software (MultiD, Sweden). RT–qPCR data analysis was done using the 2<sup>-Δ</sup>-(ddct)-method.

### 2.6 Cardiomyocyte isolation

Mice were heparinized (500 IU/kg body weight), and anaesthetized with 5% isoflurane prior to cervical dislocation. Hearts were excised and the aorta was rapidly cannulated. Mouse and human ventricular cardiomyocytes were isolated by a standard liberase-based dissociation procedure using Langendorff perfusion protocol as described previously.<sup>9,16</sup>

### 2.7 Subcellular $\text{Ca}^{2+}$ imaging and cardiomyocyte shortening

Intracellular  $\text{Ca}^{2+}$  stores were visualized in cardiomyocytes loaded with 10  $\mu\text{M}$  Mag-fluo-4/AM (Life Technologies, Grand Island, NY, USA) using a confocal imaging system (Zeiss LSM 510 Meta).<sup>9</sup>  $\text{Ca}^{2+}$  transients were recorded in cardiomyocytes loaded with 5  $\mu\text{M}$  Indo-1/AM or 8  $\mu\text{M}$  Fluo-4/AM (both Thermo Fisher Scientific, Vienna, Austria).<sup>2,9,10</sup> Indo-1-loaded and field-stimulated cardiomyocytes were subjected to a stress protocol to simulate an increased physiological workload. Cells were first paced at 0.5 Hz (baseline) followed by administration of 30 nM isoprenaline and a subsequent increase of the stimulation frequency to 5 Hz for 3 min. Stimulation rate was then set back to 0.5 Hz and isoprenaline was washed out.  $\text{Ca}^{2+}$  signals were acquired using a customized IonOptix system (Ionoptix, Dublin, Ireland).<sup>17</sup> In a subset of dye-free cardiomyocytes that were subjected to the stress protocol, contraction was assessed using a SarLen Sarcomere Length Acquisition Module (MyoCam-S, IonOptix, Dublin, Ireland) at the acquisition rate of 240 Hz. At least 10 consecutive beats were averaged and analysed using IonWizard Software (IonOptix, Dublin, Ireland). Simultaneous imaging of nucleoplasmic and cytoplasmic  $\text{Ca}^{2+}$  transients was done in Fluo-4/AM-loaded cardiomyocytes using confocal microscopy as described.<sup>9</sup> A subset of cardiomyocytes was acutely exposed to 10 nM isoprenaline to

measure the response to  $\beta$ -adrenergic stimulation. Frequency-dependent changes in  $\text{Ca}^{2+}$  cycling were assessed by gradually increasing stimulation rate from 1 to 4 Hz (mouse) or from 0.25 to 1 Hz (human). Cytoplasmic and nucleoplasmic fluorescence signals were transformed into calibrated  $[\text{Ca}^{2+}]$ .<sup>18</sup>  $\text{Ca}^{2+}$  spark were recorded in line-scan mode at a sampling rate of 1.54 or 1.92 ms per line within 30 s after the cessation of stimulation at 4 Hz, and analysed with ImageJ plugin SparkMaster (NIH, Bethesda, USA).<sup>19</sup>  $\text{Ca}^{2+}$  spark frequency was normalized to cell length and recording time, meanwhile RyR2-mediated  $\text{Ca}^{2+}$  leak was calculated as described previously.<sup>20</sup>

## 2.8 Mitochondrial redox state measurements

The mitochondrial redox state of NAD(P)H/NAD(P)<sup>+</sup> and FADH<sub>2</sub>/FAD was quantified as the autofluorescence of NAD(P)H and FAD, which was recorded in the same cell using excitation/emission wavelengths of 340/450 nm for NAD(P)H and 485/525 nm for FAD. Calibration was performed at the end of every experiment with the mitochondrial uncoupler FCCP (5  $\mu\text{M}$ ) and the complex IV inhibitor Na-cyanide (4 mM). Alternatively, the mitochondrial membrane potential ( $\Delta\Psi_m$ ) was determined with 100 nM TMRM using excitation/emission wavelengths of 540/605 nm. For the semi-quantitative assessment of  $\Delta\Psi_m$ , TMRM fluorescence was determined before and after the administration of 5  $\mu\text{M}$  FCCP and 1.25  $\mu\text{M}$  oligomycin, which is known to completely dissipate  $\Delta\Psi_m$ .<sup>21</sup>

## 2.9 Respiration measurements in isolated cardiac mitochondria

Freshly isolated cardiac mitochondria were used for high-resolution respirometry measurements that were performed as described previously.<sup>21</sup> Oxygen consumption was assayed at 37°C with an Oxygraph-2k high-resolution respirometer and DatLab software was used for data acquisition and analysis (Oroboros Instruments, Innsbruck, Austria). Two mitochondrial respiration protocols were used to quantify oxygen consumption rate upon supplementation of pyruvate (for carbohydrate metabolism) or fatty acids (for  $\beta$ -oxidation) as a fuel. In the 'carbohydrate' protocol, measurements of complex I and II activity were performed with 5 mM Na-pyruvate and 5 mM Na-malate. The metabolites were added as reduced substrates after initially recording residual oxygen consumption resulting in leak respiration, followed by increasing concentrations of ADP (0.03, 0.1, 0.3, 1 mM). Complex I was inhibited by 0.5  $\mu\text{M}$  rotenone to prevent reverse electron flux. Finally, oxygen consumption coupled to ADP phosphorylation was inhibited by adding 1.25  $\mu\text{M}$  oligomycin, followed by titration with 10  $\mu\text{M}$  DNP to determine uncoupled respiration state 3u. In the 'fatty acid' protocol, respiration was measured using 1 mM carnitine, 3 mM malate, 10  $\mu\text{M}$  palmitoyl-CoA, 10  $\mu\text{M}$  oleoyl-L-carnitine. Similar to the 'carbohydrate' protocol, increasing amounts of ADP, 1.25  $\mu\text{M}$  oligomycin or 10  $\mu\text{M}$  DNP were added. Mitochondrial membrane potential was simultaneously probed using 1  $\mu\text{M}$  TMRM and Smart Fluo-Sensor Green, as described before.<sup>21</sup>

## 2.10 Immunocytochemistry

Immunocytochemistry was performed using antibodies against SERCA2a (A010-20, Badrilla), RyR2 (MA3-925, Thermo Fisher Scientific) and phospho-Thr286-CaMKII (ab32678, Abcam).<sup>9</sup> Western blotting and detailed immunostaining analyses were used to validate the specificity of antibodies. Cells pretreated with KN-93 served as a negative control for anti-phospho-Thr286-CaMKII antibody; meanwhile *bona*

*fide* target staining was distinguished from the background by staining with a suitable secondary antibody alone.

## 2.11 Western blotting

Hearts were perfused with normal Tyrode solution containing or not 10 nM isoprenaline for 5 min, and were then flash frozen for further immunoblotting with primary antibodies recognizing ATG5, SERCA2a, phospholamban (PLB), Troponin I, phospho-PLB-Ser16, phospho-Troponin I-Ser23/24 and GAPDH (for details, see [Supplementary material online](#)).

## 2.12 Acute inhibition of autophagic flux

Autophagic flux in *Atg5*<sup>+/+</sup> animals was blocked using leupeptin-based inhibition of LC3-II (microtubule-associated protein 1 light chain 3-II) turnover, as described previously.<sup>22</sup> *Atg5*<sup>+/+</sup> mice received intraperitoneal injections of leupeptin (40 mg/kg body weight, Sigma-Aldrich, Vienna, Austria) or vehicle (sterile 0.9% NaCl solution), and were sacrificed 50 min after the injection. Isolated cardiomyocytes were subjected to subcellular  $\text{Ca}^{2+}$  imaging and immunoblot analysis of LC3 and p62/SQSTM1.

## 2.13 Design-based stereology

Hearts were retrogradely perfused with 4% neutral-buffered formaldehyde and processed for the quantification of LV cardiomyocyte composition using electron microscopy and design-based stereology as described elsewhere.<sup>4</sup>

## 2.14 Statistical analysis

Statistical testing was performed using GraphPad Prism 8 (GraphPad Software, CA). Data are presented as bar graphs with error bars showing mean and SEM, respectively, with single data points superimposed. Indicated sample size was determined based on the means and variance of the studied parameters in our previous work on disease mouse models and failing human hearts.<sup>9,10</sup> Data residuals distribution was determined using Shapiro-Wilk's test, while homogeneity of variance was verified by Bartlett's test. Comparisons between two groups were analysed using Student's *t*-test or Mann-Whitney test, as appropriate. In case of multiple comparisons, ANOVA with Dunnett's or Bonferroni's *post hoc* test was applied. In case of  $\text{Ca}^{2+}$  transient measurements at different stimulation frequencies or time-lapse/serial measurements, two-way repeated measures ANOVA was used. Significant factorial designs were followed by multiple comparisons using Sidak's or Bonferroni's *post hoc* test. Association of *Atg5* gene and ATG5 protein expression levels to interventricular septum was tested using Pearson correlation. Differences were considered significant, if two-tailed *P*-value was less than 0.05.

# 3. Results

## 3.1 Reduced expression of ATG5 and autophagy markers in human hearts with compensated hypertrophy and heart failure

Given that acute pressure overload reduces ATG5 expression and overall pro-autophagic flux in mice,<sup>23</sup> we assessed the clinical relevance of these findings by quantifying gene and protein expression of ATG5 in human left ventricular (LV) biopsies of non-failing, hypertrophied, and failing

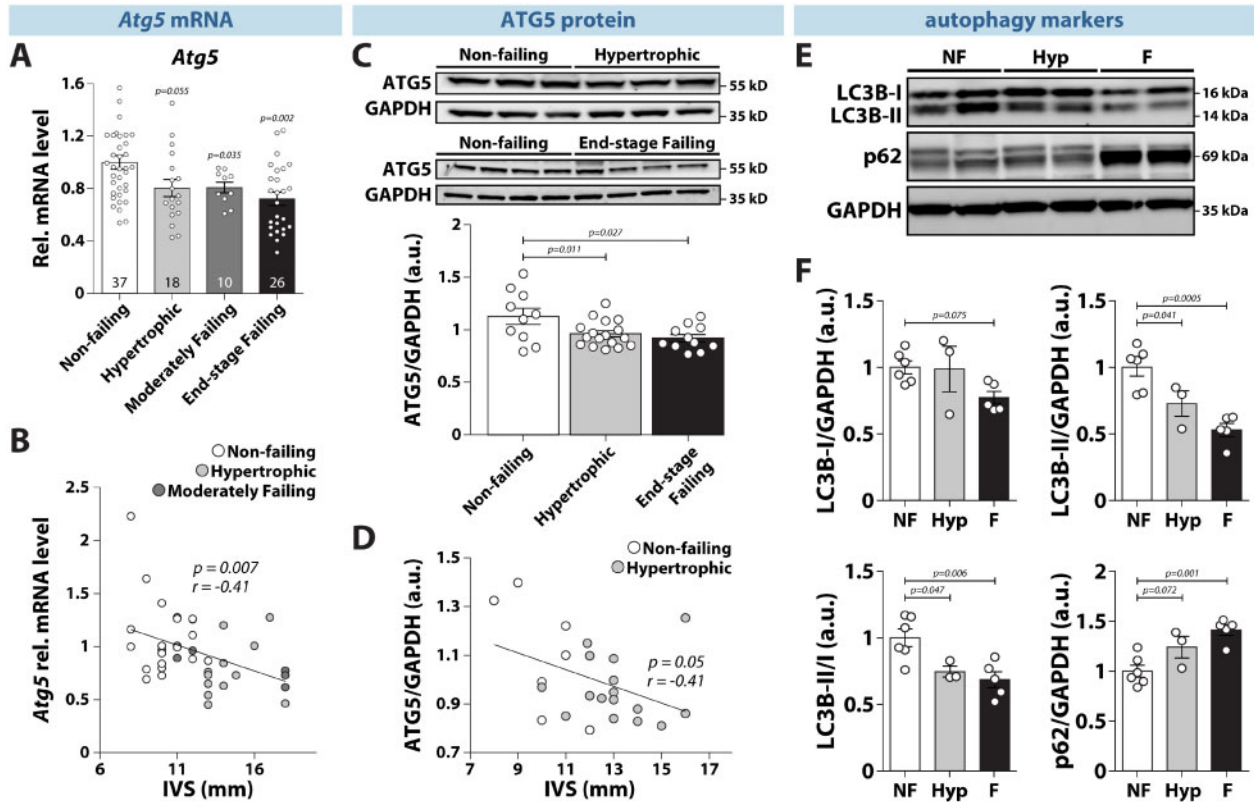


**Figure 1** Reduced gene and protein expression of Atg5 and impaired cardiac autophagy in hypertrophic and failing human hearts. (A) ATG5 expression in left ventricular tissue from non-failing, hypertrophied, moderately failing and end-stage failing human myocardium. Number of hearts per group is shown in each bar. (B) Regression analysis of ATG5 expression levels and thickness of interventricular septum (IVS) from non-failing, hypertrophied, and moderately failing human hearts ( $N = 23/12/6$  hearts, respectively). (C) ATG5 protein expression in left ventricular tissue from non-failing, hypertrophied, and end-stage failing human ventricular tissue ( $N = 10/17/11$  hearts, respectively). (D) Regression analysis of ATG5 protein expression levels and thickness of the interventricular septum (IVS) from non-failing and hypertrophied human hearts ( $N = 7/16$  hearts, respectively). (E) Representative original immunoblots and, (F) expression of the autophagy-related protein markers in non-failing (NF), hypertrophied (Hyp), and end-stage failing hearts (F) ( $N = 6/3/5$  hearts, respectively). (A–F) Data show mean  $\pm$  SEM. Indicated  $P$ -values were calculated using ANOVA followed by Dunnett's *post hoc* test. (B) and (D) Association of Atg5 gene and ATG5 protein expression with IVS thickness was computed using Pearson correlation.

hearts from donors, who underwent echocardiographic examination prior to heart extraction (Supplementary material online, Figure S1). Importantly, both Atg5 gene and protein expression were significantly reduced in hypertrophied and failing human hearts as compared to non-failing controls (Figure 1A and C). Furthermore, mRNA and protein expression of ATG5 inversely correlated with the thickness of the interventricular septum, a measure of cardiac hypertrophy (Figure 1B and D). Notably, ATG5 down-regulation during early and late LV remodelling coincided with a decreased LC3B-II expression and LC3B-II/LC3B-I ratio, and an increased expression of p62/SQSTM1 in hypertrophied and failing myocardium (Figure 1E and F). These results indicate that decreased Atg5 gene and protein expression along with the reduced amount of autophagy markers appear as an early event in human cardiac remodelling, likely contributing to its transition towards heart failure.

### 3.2 Atg5<sup>-/-</sup> mice exhibit reduced contractility and exercise capacity in response to stress

To assess the effect of myocardial Atg5 deficiency on cardiac function *in vivo*, we performed baseline and acute  $\beta$ -adrenergic stress testing in

Atg5<sup>-/-</sup> mice before the development of congestive heart failure. These mice had inhibited cardiomyocyte autophagy (Supplementary material online, Figure S2), which was associated with a mild increase in hypertrophy, as determined by elevated heart-to-body weight ratio and myocardial NppB gene expression (Figure 2A–C). At baseline, Atg5-deficient mice showed no cardiac abnormalities (Supplementary material online, Table S4), as also denoted by similar heart rates (Figure 2D) and systolic function, measured invasively by maximal LV pressure development rate (dPdt<sub>max</sub>) (Figure 2E). Isoprenaline administration expectedly evoked increased heart rate and contractility in both groups. However, the increase in dPdt<sub>max</sub> upon isoprenaline was lower in Atg5<sup>-/-</sup> mice than in control animals (Figure 2E), despite similar maximum heart rate development (Figure 2D), indicating reduced cardiac reserve capacity. To examine the outcome of such attenuated inotropic response in the physiological context of increased cardiac demand, we exposed Atg5-deficient mice to exercise tolerance testing. Atg5<sup>+/+</sup> and Atg5<sup>-/-</sup> mice displayed a similar level of exhaustion as determined by comparable blood lactate concentrations ( $15 \pm 6$  and  $17.3 \pm 5.7$  mM, respectively;  $P = 0.45$ ). However, Atg5<sup>-/-</sup> mice reached exhaustion faster than control mice and, thus, had shorter maximum run distance (Figure 2F). Most

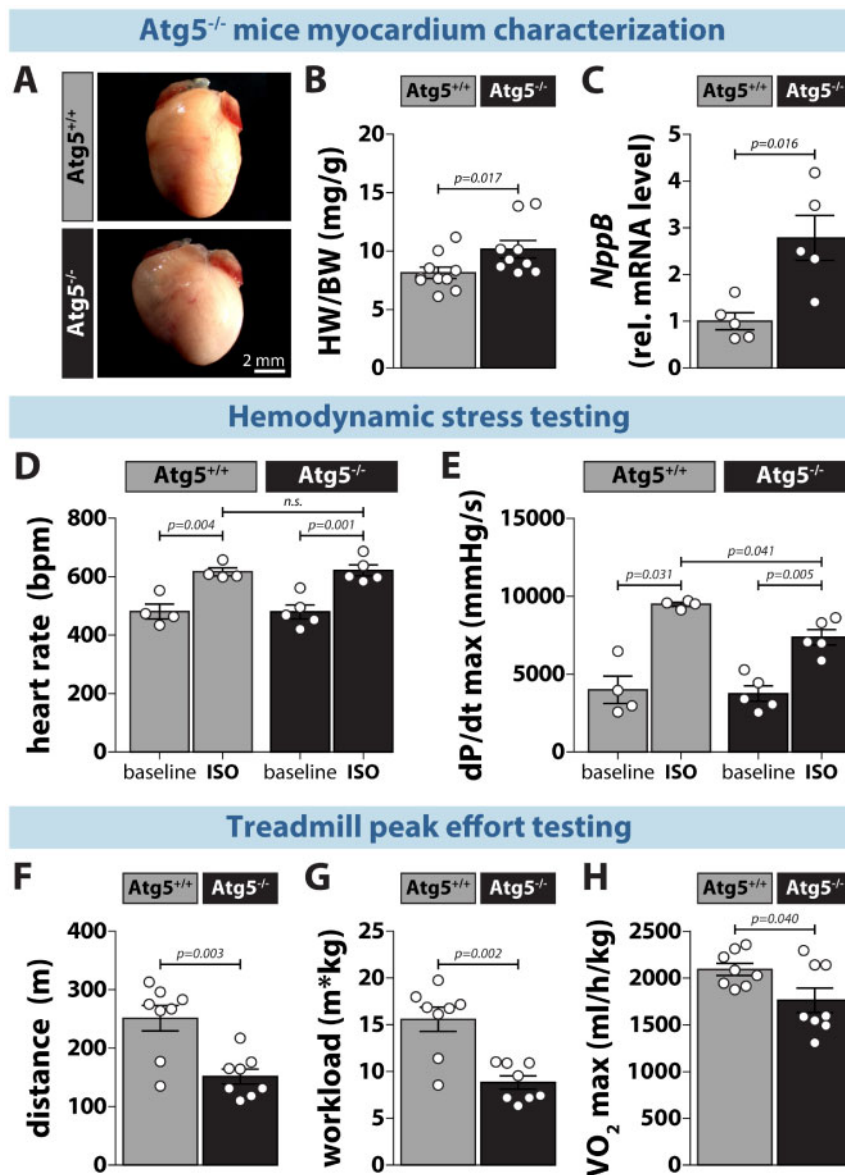


**Figure 2** *Atg5*-depleted mice exhibit mild hypertrophy, reduced cardiac contractility and exercise capacity. (A) Photomicrographs of hearts from 12-week-old *Atg5<sup>+/+</sup>* (left) and *Atg5<sup>-/-</sup>* mice (right). (B) Heart weight-to-body weight ratio (HW/BW) and, (C) *NppB* expression in *Atg5<sup>+/+</sup>* vs. *Atg5<sup>-/-</sup>* hearts (*N* = 10 vs. 9 mice for HW/BW, and *N* = 5 mice per group for *NppB* expression). (D) Heart rate (bpm, beats per minute) and, (E) maximal positive pressure development (dP/dt<sub>max</sub>) in the left ventricle at baseline and upon intraperitoneal administration of isoprenaline (ISO, 2 μg/kg body weight) in *Atg5<sup>+/+</sup>* and *Atg5<sup>-/-</sup>* mice. *N* = 4/5 mice, respectively. (F) Maximal run distance, (G) workload and, (H) maximal oxygen consumption (VO<sub>2</sub>max) in *Atg5<sup>-/-</sup>* mice and their control littermates during peak effort testing on a motorized treadmill coupled to indirect calorimetry. *N* = 8 mice per group. (B–H) Data show mean ± SEM. Indicated *P*-values were calculated using Mann–Whitney test comparing *Atg5<sup>-/-</sup>* or ISO treatment to the respective control.

importantly, *Atg5<sup>-/-</sup>* mice had significantly reduced total workload (Figure 2G), which coincided with lower maximal aerobic capacity (Figure 2H), collectively indicating effort intolerance.

### 3.3 Preserved Ca<sup>2+</sup> homeostasis in *Atg5<sup>-/-</sup>* cardiomyocytes during baseline and β-adrenergic stimulation

Since intracellular Ca<sup>2+</sup> homeostasis is the major determinant of excitation–contraction coupling and, thus, determines cardiac performance,

we evaluated the functional impact of impaired ATG5-dependent autophagy on intracellular Ca<sup>2+</sup> handling by quantifying cytosolic and nuclear Ca<sup>2+</sup> transients under normal and stressed conditions. At baseline, Indo-1 wide-field and Fluo-4 confocal imaging revealed similar intracellular Ca<sup>2+</sup> concentrations ([Ca<sup>2+</sup>]<sub>i</sub>) at diastole and systole, as also kinetic parameters in both groups (Figure 3A–F). As alterations in Ca<sup>2+</sup> cycling occur rapidly during sympathetic activation, β-adrenergic stimulation might unmask subtle changes that are indiscernible at baseline. To that end, we investigated whether acute isoprenaline exposure alters intracellular Ca<sup>2+</sup> handling in *Atg5*-depleted cardiomyocytes. While

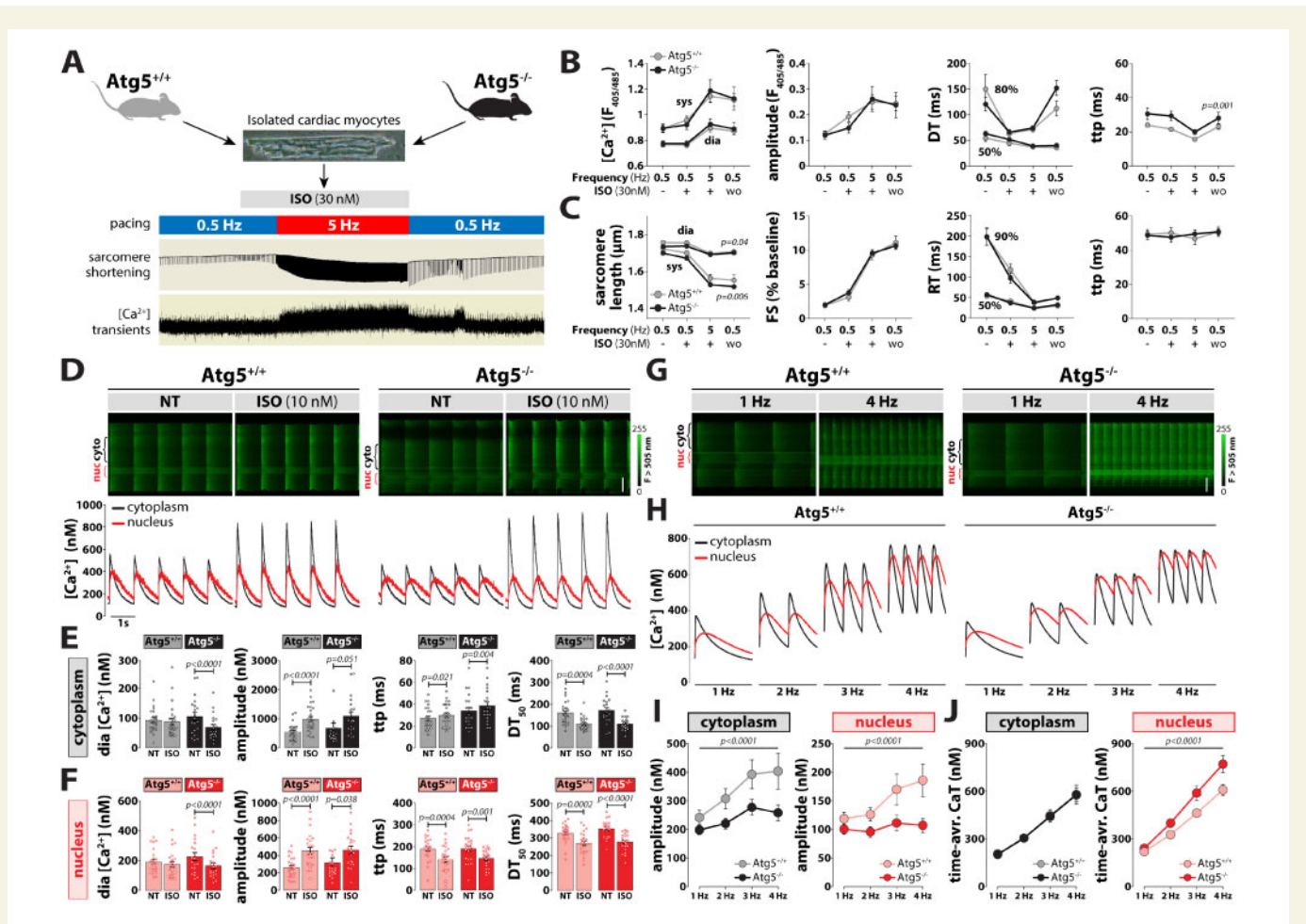


**Figure 3** Impaired subcellular  $\text{Ca}^{2+}$  cycling in response to increased workload in  $\text{Atg5}^{-/-}$  cardiomyocytes. (A) Schematic representation of the stress protocol that simulates increased physiological workload by increasing stimulation frequency from 0.5 to 5 Hz during exposure to 10 nM isoprenaline (ISO). (B) Quantification of global calcium transients using Indo-1/AM. From left to right: Systolic and diastolic  $[\text{Ca}^{2+}]_i$ , amplitude, decay time (DT) and time-to-peak (ttp) in isolated cardiac myocytes subjected to a physiological stress protocol (A). Data show mean  $\pm$  SEM.  $n = 28/18$  cells from 3/2  $\text{Atg5}^{+/+}/\text{Atg5}^{-/-}$  mice, respectively. (C) Quantification of myocyte contractility in unstained cells using the stress protocol in (A). From left to right: Sarcomere length, fractional shortening (FS), relaxation time (RT) and time-to-peak (ttp). Data show mean  $\pm$  SEM ( $n = 35/32$  cells from 3/3  $\text{Atg5}^{+/+}/\text{Atg5}^{-/-}$  mice, respectively). (D) Original line-scan Fluo-4/AM fluorescence recordings (top) of intracellular  $\text{Ca}^{2+}$  transients at baseline and upon acute administration of 10 nM isoprenaline (ISO) in a representative control (left) and  $\text{Atg5}$ -deficient (right) cardiomyocyte, and corresponding calibrated cytoplasmic (black) and nucleoplasmic (red)  $\text{Ca}^{2+}$  transients (bottom). Scale bar, 20  $\mu\text{m}$ . Mean values of cytoplasmic (E) and nucleoplasmic (F)  $\text{Ca}^{2+}$  transient parameters displaying diastolic (dia)  $[\text{Ca}^{2+}]_i$ ,  $\text{Ca}^{2+}$  transient amplitude, time-to-peak (ttp), and time from peak  $[\text{Ca}^{2+}]_i$  to 50% decline ( $\text{DT}_{50}$ ). Data show mean  $\pm$  SEM ( $n = 24/20$ –22 cells from 5/4  $\text{Atg5}^{+/+}/\text{Atg5}^{-/-}$  mice, respectively). (G) Original line-scan confocal images of cytoplasmic and nucleoplasmic  $\text{Ca}^{2+}$  transients at 1 and 4 Hz stimulation in a ventricular myocyte isolated from  $\text{Atg5}^{+/+}$  (left) and  $\text{Atg5}^{-/-}$  (right) mice. Note the area of increased fluorescence intensity displaying increased nuclear  $\text{Ca}^{2+}$  (nuc). Scale bar, 20  $\mu\text{m}$ . (H) Averaged original recordings of electrically stimulated  $\text{Ca}^{2+}$  transients in the nucleus (red) vs. cytoplasm (black) of ventricular myocytes isolated from  $\text{Atg5}^{+/+}$  (left) and  $\text{Atg5}^{-/-}$  (right) mice in response to a gradual increase of stimulation frequency from 1 to 4 Hz. (I) Frequency-dependent changes in peak systolic amplitude in electrically stimulated  $\text{Ca}^{2+}$  transient in the cytoplasm (left) vs. nucleus (right) of ventricular myocytes isolated from control and  $\text{Atg5}$ -deficient mice. (J) Cytoplasmic (left) and nucleoplasmic (right)  $\text{Ca}^{2+}$  load was calculated as a time-integral area under  $\text{Ca}^{2+}$  transient-time curve within 1 s in  $\text{Atg5}^{+/+}$  and  $\text{Atg5}^{-/-}$  cardiomyocytes. (H–J) Data show mean  $\pm$  SEM ( $n = 19/25$  cells from 3/3  $\text{Atg5}^{+/+}/\text{Atg5}^{-/-}$  mice, respectively). (B and C) and (I and J)  $P$ -values were calculated using Bonferroni's or Sidak's *post hoc* test (vs.  $\text{Atg}^{+/+}$  control), following significant two-way repeated-measures ANOVA. (E and F)  $P$ -values were calculated using Mann–Whitney test comparing  $\text{Atg5}^{-/-}$  or ISO to the respective control. Average data and group comparisons related to Figure 3 are summarized in [Supplementary material online, Table S5](#).

isoprenaline increased the amplitude and reduced the decay time of global  $\text{Ca}^{2+}$  transients similarly in both groups (Figure 3A–F),  $\text{Atg5}^{-/-}$  cardiac myocytes displayed reduced sarcomere length during diastole and systole, which coincided with normal fractional shortening and contractile kinetics (Figure 3C), suggesting an early onset of diastolic dysfunction

in  $\text{Atg5}^{-/-}$  mice. We showed previously that nucleoplasmic and cytoplasmic  $\text{Ca}^{2+}$  homeostasis can be regulated independently, and that nucleoplasmic  $\text{Ca}^{2+}$  signalling is an early contributor to the development of cardiac hypertrophy.<sup>9</sup> However, at slow pacing rates  $\text{Atg5}^{-/-}$  cardiomyocytes displayed preserved nucleoplasmic and

cytoplasmic  $\text{Ca}^{2+}$  handling at baseline and upon isoprenaline administration (Figure 3D–F), indicating that subcellular  $\text{Ca}^{2+}$  handling was preserved during normal and stressed conditions despite the loss of Atg5-dependent autophagy.

### 3.4 Impaired subcellular $\text{Ca}^{2+}$ cycling and signalling in $\text{Atg5}^{-/-}$ mice at high-pacing frequencies

Unlike *in vitro*,  $\beta$ -adrenergic stimulation *in vivo* exerts multiple effects on the heart, including positive inotropy and chronotropy. Therefore, we assessed the impact of Atg5 deficiency at high heart rates by exposing cardiomyocytes to increasing pacing frequencies (1–4 Hz), but in the absence of isoprenaline. Notably, the frequency-dependent increase in peak systolic  $\text{Ca}^{2+}$  amplitude that was observed in  $\text{Atg5}^{+/+}$  cells was blunted in  $\text{Atg5}^{-/-}$  cardiomyocytes in both the cytoplasm and nucleus (Figure 3G–I). However, although the time-averaged cytoplasmic  $\text{Ca}^{2+}$  transient was identical between  $\text{Atg5}^{-/-}$  and  $\text{Atg5}^{+/+}$ , time-averaged nucleoplasmic  $\text{Ca}^{2+}$  load was elevated in Atg5-deficient cells (Figure 3J). Such increase in nucleoplasmic  $[\text{Ca}^{2+}]$  is known to activate  $\text{Ca}^{2+}$ /calmodulin-dependent protein kinase II (CaMKII) at high-pacing frequencies and stimulate cardiomyocyte growth,<sup>24</sup> as indicated by increased cell and nucleus width-to-length ratio (Supplementary material online, Figure S3). Therefore, we opted to measure CaMKII phosphorylation in  $\text{Atg5}^{-/-}$  cardiomyocytes subjected to 1 and 4 Hz stimulation. Although the extent of CaMKII phosphorylation was comparable in the cytoplasm and nucleoplasm between  $\text{Atg5}^{-/-}$  and  $\text{Atg5}^{+/+}$  cells, CaMKII activation was more pronounced on the nuclear envelope of  $\text{Atg5}^{-/-}$  cardiomyocytes already at low pacing rates as compared to control cells (Figure 4D). At high frequencies, CaMKII phosphorylation was elevated also in the cytoplasm and nucleoplasm of  $\text{Atg5}^{-/-}$  cells (Figure 4A–C). To examine whether acute or chronic autophagy inhibition impairs subcellular  $\text{Ca}^{2+}$  handling, we then acutely blocked autophagic flux in  $\text{Atg5}^{+/+}$  mice, as

determined by LC3 and p62 immunoblotting after blocking lysosome function with intraperitoneal injection of leupeptin (Supplementary material online, Figure S4). Pharmacological autophagy inhibition failed to elicit direct changes in time-averaged  $\text{Ca}^{2+}$  transients in the cytoplasm and nucleoplasm. Therefore, loss of Atg5-dependent autophagy seems to induce adverse cardiac remodelling that involves increased CaMKII activity due to the imbalances in nuclear  $[\text{Ca}^{2+}]$ .

### 3.5 Atg5 deficiency does not alter intracellular $\text{Ca}^{2+}$ stores but reduces the phosphorylation of troponin I

Because sarcoplasmic reticulum (SR) is the major determinant of the  $\text{Ca}^{2+}$  transient in cardiomyocytes, we examined whether Atg5 deficiency alters the properties of the SR and, consequently, has an impact on the SR  $\text{Ca}^{2+}$  load and/or spontaneous SR  $\text{Ca}^{2+}$  release. To this end, we performed imaging of  $\text{Ca}^{2+}$  in intracellular stores, which revealed no organizational alterations or fragmentation of the SR or NE, and no obvious reduction in the ability of Mag-Fluo-4 to diffuse through the SR and NE lumen (Supplementary material online, Figure S5A), suggesting that both intracellular  $\text{Ca}^{2+}$  stores were efficiently connected in  $\text{Atg5}^{-/-}$  cardiomyocytes. This finding was corroborated with a similar SR  $\text{Ca}^{2+}$  load in  $\text{Atg5}^{-/-}$  and  $\text{Atg5}^{+/+}$  cardiomyocytes, as assessed by the peak amplitude of the caffeine-induced  $\text{Ca}^{2+}$  transient (Supplementary material online, Figure S5B). Loss of ATG5 also failed to increase RyR2-mediated SR  $\text{Ca}^{2+}$  leak measured as a product of  $\text{Ca}^{2+}$  spark frequency and  $\text{Ca}^{2+}$  spark mass (Supplementary material online, Figure S5C). These effects coincided with unaltered expression of SR  $\text{Ca}^{2+}$  ATPase 2a (SERCA2a) and phosphorylation of its main regulator phospholamban (PLB) between both groups, meanwhile phosphorylation of troponin I (TnI) at serines 23/24 was significantly reduced in  $\text{Atg5}^{-/-}$  mice as compared to controls (Figure 5A–D). To assess the effect of acute  $\beta$ -adrenergic stimulation on PLB and TnI phosphorylation, we then perfused a subset of mouse hearts *ex vivo* with 10 nM isoprenaline. As isoprenaline only moderately augments the beat rate of *ex vivo* perfused hearts,<sup>25</sup> the effects of frequency-mediated  $\beta$ -adrenergic signalling *in vivo* are essentially blunted. Hence, this approach enabled us to study primarily the impact of protein kinase A (PKA)-dependent phosphorylation on PLB and TnI. Notably, isoprenaline-perfused hearts of  $\text{Atg5}^{+/+}$  and  $\text{Atg5}^{-/-}$  mice displayed increased PLB and TnI phosphorylation (Figure 5B, C, and E). However, despite fully preserved PLB phosphorylation, Atg5-deficient hearts showed a markedly attenuated increase in PKA-dependent phosphorylation of TnI at serines 23/24 (Figure 5E).

### 3.6 Reduced abundance of mitochondria leads to their functional overcompensation in $\text{Atg5}^{-/-}$ mice

Both reduced TnI phosphorylation and blunted increase of  $\text{Ca}^{2+}$  transient amplitude at high-pacing frequencies contribute to the reduction of systolic function in  $\text{Atg5}^{-/-}$  mice under conditions of increased cardiac demand. This may result from mitochondrial abnormalities, such as reduced respiratory activity,<sup>5</sup> and/or impaired cardiomyocyte composition. Therefore, we systematically assessed the structural characteristics and quantified ultrastructural composition of Atg5-deficient cardiomyocytes. Unlike in  $\text{Atg5}^{+/+}$  cells (Figure 6A and B), we observed accumulation of concentric layers of membrane sheaths as well as cisternae of membranes resembling SR (Figure 6C and D) in the sarcoplasm of autophagy-incompetent cardiomyocytes. In addition, myofibrillar disarray and atypical aggregates of mitochondria were clearly distinguishable (Figure 6E and

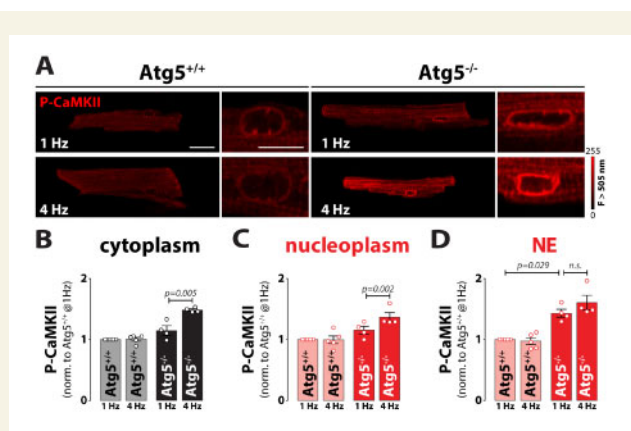


**Figure 4** Intact intracellular  $\text{Ca}^{2+}$  stores and impaired  $\text{Ca}^{2+}$  signalling in response to increased workload in Atg5-deprived hearts. (A) Representative fluorescent images of cardiomyocytes isolated from  $\text{Atg5}^{+/+}$  and  $\text{Atg5}^{-/-}$  mice immunostained against phospho-CaMKII at 1 or 4 Hz stimulation frequency. Scale bar indicates 20  $\mu\text{m}$  for whole cell images or 10  $\mu\text{m}$  for magnified images of the nucleus. (B) Mean cytosolic, (C) nucleoplasm and, (D) nuclear envelope (NE) fluorescence values normalized to  $\text{Atg5}^{+/+}$  control cardiomyocytes paced at 1 Hz. Data show mean  $\pm$  SEM ( $n = 153/159$  cells from 5/4  $\text{Atg5}^{+/+}/\text{Atg5}^{-/-}$  mice, respectively). Indicated  $P$ -values were calculated using Mann–Whitney test comparing  $\text{Atg5}^{-/-}$  or 4 Hz to the respective control.



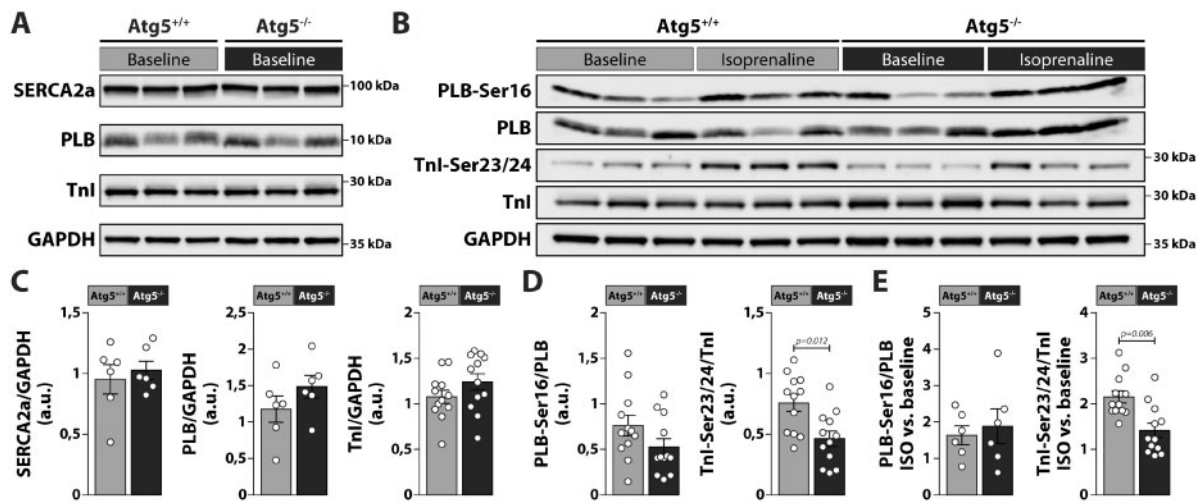


**Figure 5** Expression and phosphorylation of  $\text{Ca}^{2+}$ -regulatory proteins in *Atg5*-deprived hearts. (A and B) Representative original immunoblots and, (C–E) densitometric analysis of expression and phosphorylation of  $\text{Ca}^{2+}$ -regulatory proteins in lysates from *Atg5*<sup>+/+</sup> and *Atg5*<sup>-/-</sup> mouse hearts in the absence or presence of ISO. From left to right: total SERCA2a, phospholamban (PLB) and Troponin I (Tnl), PLB phosphorylated on serine at site 16 (PLB-Ser16), Tnl phosphorylated on serine at sites 23 and 24 (Tnl-Ser23/24), and relative increase in PLB and Tnl phosphorylation upon isoprenaline (ISO) administration are shown. Data show mean  $\pm$  SEM of  $N = 6$ –12 samples per group, indicated  $P$ -values were calculated using Mann–Whitney test comparing *Atg5*<sup>-/-</sup> and *Atg5*<sup>+/+</sup>.

F). *Atg5*<sup>-/-</sup> cardiomyocytes had slightly, but significantly increased volume of myofibrils (Figure 6G) and decreased total and also individual mitochondrial volume (i.e. volume-weighted mean volume of mitochondria) (Figure 6H and J), resulting in reduced mitochondrial abundance and myofibril-to-mitochondria relative volume ratio (Figure 6I).

Atypical accumulation of mitochondria with decreased volume prompted us to test the functional properties of cardiac mitochondria from *Atg5*<sup>-/-</sup> mice. Surprisingly, we found no difference in oxygen consumption rate and mitochondrial membrane potential ( $\Delta\Psi_m$ ) upon pyruvate or fatty acids supplementation between both groups (Supplementary material online, Figure S6). As a considerable fraction of dysfunctional mitochondria can be lost during mitochondria isolation by gradient centrifugation, we assessed mitochondrial redox state in intact *Atg5*<sup>-/-</sup> cardiomyocytes using a physiological stress protocol (Figure 3A). Despite preserved mitochondrial membrane potential (Figure 6K), the overall redox state, measured as the NAD(P)H/FAD fluorescence intensity ratio, was increased in *Atg5*<sup>-/-</sup> cardiomyocytes (Figure 6L and M). Furthermore, absolute fluorescence intensities of NAD(P)H and FAD were comparable between both groups (NAD(P)H:  $1404 \pm 105$  a.u. vs.  $1432 \pm 63$  a.u.,  $P = 0.82$ ; FAD:  $270 \pm 21$  a.u. vs.  $270 \pm 15$ ,  $P = 0.99$ ; respectively). However, considering that *Atg5*-deficient cardiomyocytes were hypertrophied and had reduced mitochondrial volume, these results suggest that individual mitochondria are likely in an overcompensated state, which can lead to mitochondrial exhaustion and energy deficit, especially under increased workload.

### 3.7 Human cardiomyocytes from hypertrophied hearts phenocopy impaired subcellular $\text{Ca}^{2+}$ cycling in *Atg5*<sup>-/-</sup> cardiomyocytes

Finally, we tested whether reduced ATG5 expression in hypertrophied human myocardium (Figure 1A and C) is related to alterations in  $\text{Ca}^{2+}$

handling, which resemble those in *Atg5*<sup>-/-</sup> mice. Indeed, human cardiomyocytes displayed blunted frequency-dependent increase of  $\text{Ca}^{2+}$  amplitude and increased nucleoplasmic  $\text{Ca}^{2+}$  load at higher pacing frequencies (Figure 7A–D). As  $\beta$ -adrenergic stimulation accelerates  $\text{Ca}^{2+}$  transient decay and improves frequency-dependent changes in  $\text{Ca}^{2+}$  cycling,<sup>26</sup> we hypothesized that isoprenaline diminishes or even prevents the disturbances of  $\text{Ca}^{2+}$  cycling in hypertrophied cardiomyocytes exposed to increasing pacing frequencies alone. Isoprenaline expectedly provoked a robust increase of both nucleoplasmic and cytoplasmic  $\text{Ca}^{2+}$  transients in both non-failing and hypertrophied cardiomyocytes. Interestingly, the increase in peak amplitude was preserved in hypertrophied compared to control cells at high-stimulation frequencies only in the presence of isoprenaline (Figure 7E–G), indicating an overproportioned reliance on  $\beta$ -adrenergic stimulation. Overall, frequency-dependent changes of subcellular  $\text{Ca}^{2+}$  transients in hypertrophied human cardiomyocytes were remarkably similar to those observed in *Atg5*<sup>-/-</sup> cells.

## 4. Discussion

Beta-adrenergic receptor signalling is the fundamental physiological mechanism underlying acute modulation of  $\text{Ca}^{2+}$  handling and contractility in cardiomyocytes.<sup>27</sup> However, sympathetic hyperactivity is a hallmark of heart failure development,<sup>28</sup> and previous work demonstrated that autophagy protects mice against the development of heart failure induced by chronic  $\beta$ -adrenergic stress.<sup>2</sup> Our results demonstrate that the non-selective  $\beta$ -adrenergic agonist, isoprenaline, induced only a moderately positive inotropic response in autophagy-deficient mouse hearts during increased cardiac demand. Reduced positive inotropy in *Atg5*<sup>-/-</sup> mice coincided with compromised cardiopulmonary functional reserve capacity during exercise. Our finding that reduced cardiac reserve and exercise intolerance in *Atg5*<sup>-/-</sup> mice preceded the onset of heart failure

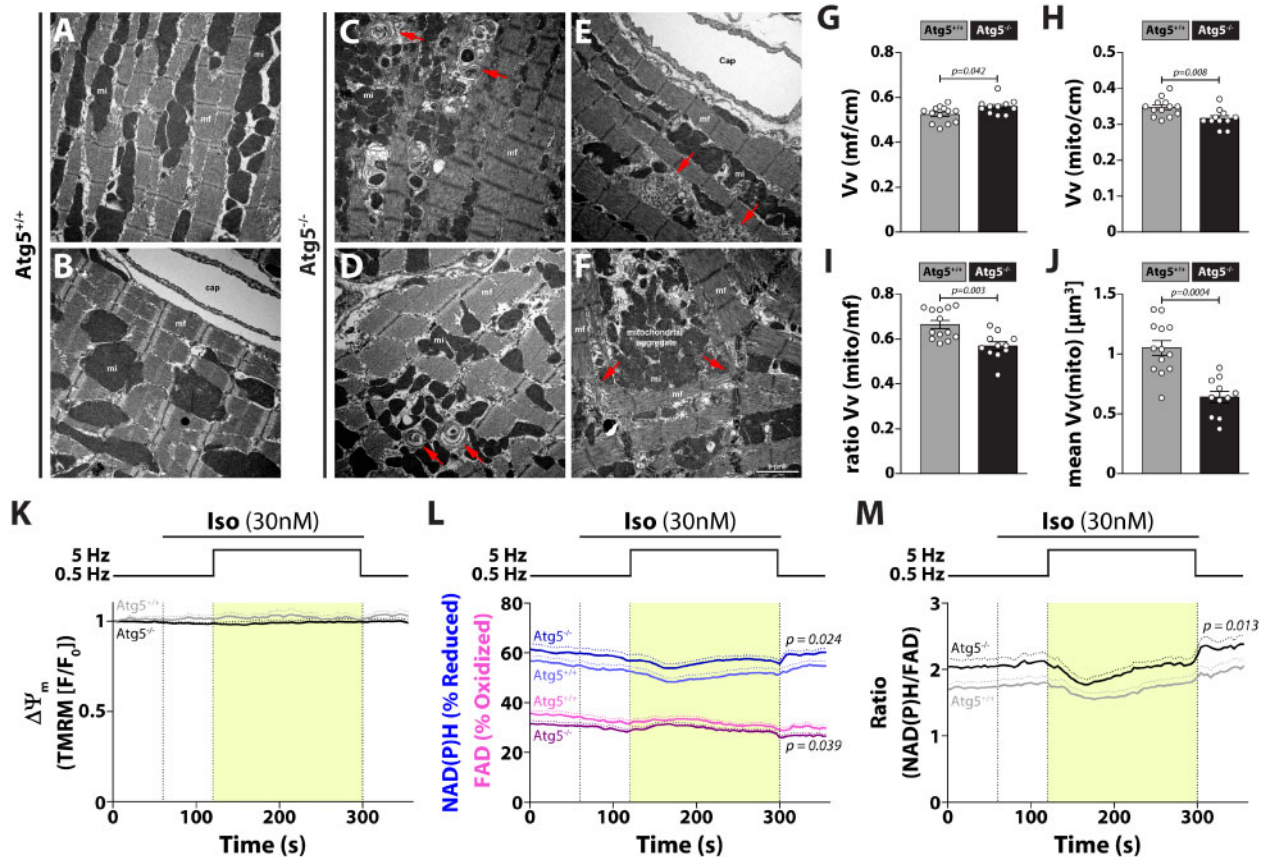


**Figure 6** *Atg5*-deficiency causes aberrant cardiomyocyte composition, decreased mitochondrial abundance and functional overcompensation of individual mitochondria. (A–F) Representative transmission electron micrographs of longitudinal sections of cardiomyocytes depict ultrastructural changes due to the absence of basal autophagy. Note onion-like membrane aggregation (red arrows in C and D), membrane cisternae (red arrows in E), sarcomere disarray, misalignment of myofibrils (red arrows in F), and aggregation of mitochondria (F). Scale bar, 2 μm; Cap, capillary; mf, myofibril; mi, mitochondria; cm, cardiomyocytes. Relative volume of (G) myofibrils Vv(mf/cm) and, (H) mitochondria Vv(mito/cm) per cardiomyocyte from *Atg5*<sup>+/+</sup> and *Atg5*<sup>-/-</sup> mouse hearts. (I) Ratio between the relative volume of mitochondria and myofibrils, Vv(mito/cm)/Vv(mf/cm). (J) Volume-weighted mean volume of mitochondria, meanVv(mi), was used to quantify mitochondrial volume and size distribution in *Atg5*<sup>+/+</sup> vs. *Atg5*<sup>-/-</sup> mouse hearts. (G–J) Data show mean ± SEM of N = 11–13 mice per group, indicated P-values were calculated using Mann–Whitney test comparing *Atg5*<sup>-/-</sup> to the *Atg5*<sup>+/+</sup> control. Isolated *Atg5*<sup>-/-</sup> and *Atg5*<sup>+/+</sup> cardiomyocytes were exposed to the stress protocol as in Figure 3A. (K) Mitochondrial membrane potential (ΔΨ<sub>m</sub>; determined by TMRM fluorescence normalized to resting fluorescence, F/F<sub>0</sub>), (L) NAD(P)H/NAD(P)<sup>+</sup> and FADH<sub>2</sub>/FAD (autofluorescence determined in the same cells) and, (M) ratio of reduced NAD(P)H to oxidized FAD (data from L) were determined. (K–M) Data show mean ± SEM, n = 28/18 cells from 3/2 *Atg5*<sup>+/+</sup>/*Atg5*<sup>-/-</sup> mice, respectively, for TMRM measurements, and n = 33/32 cells from 3/3 *Atg5*<sup>+/+</sup>/*Atg5*<sup>-/-</sup> mice, respectively, for NAD(P)H/NAD(P)<sup>+</sup> and FADH<sub>2</sub>/FAD measurements. P-values were calculated using Bonferroni's *post hoc* test, following significant two-way repeated-measures ANOVA.

might be clinically relevant as exercise capacity is known to be a major predictor of all-cause mortality.<sup>29</sup> In addition, our study demonstrates that a failure to reinstate or increase basal autophagy in the heart, and possibly also in other tissues (e.g. skeletal muscle), could be associated with the low ability of some individuals to sustain or enhance cardiac reserve in response to exercise.<sup>30</sup> Of note, physical activity is a non-pharmacological intervention that consistently re-establishes autophagic flux and mitochondrial quality control in experimental heart failure.<sup>31</sup> This underscores the importance of basal autophagy in cardiac response to acute exercise, and extends previous reports on skeletal muscle function, in which *Atg7* gene deletion was shown to compromise muscle mass, force generation and mitochondrial function.<sup>32</sup> Indeed, isoprenaline-mediated β-adrenergic stress unmasked cardiac decompensation associated with exercise intolerance, a hallmark of heart failure, arising

from cardiomyocyte abnormalities, including alterations in myofilament properties (e.g. TnI) and mitochondrial inability to maintain redox balance under acute stress. In line with this notion, aged hearts display a decline in autophagic activity, altered redox state, attenuated response to sympathetic stimulation, and reduced contractility.<sup>4</sup> In the absence of β-adrenergic stimulation, however, high-frequency pacing stunted the amplitude of Ca<sup>2+</sup> transients, while it augmented nucleoplasmic Ca<sup>2+</sup> load and CaMKII activity, especially in the nuclear region, suggesting that *Atg5* null cardiomyocytes rely considerably on β-adrenergic signalling during acute stress.

Cardiomyocyte contraction and relaxation depend on the conversion of rise and fall of cytosolic [Ca<sup>2+</sup>] into force production.<sup>27</sup> Increases in contraction and relaxation under conditions of elevated workload are primarily determined by a combination of increased SERCA2a activity

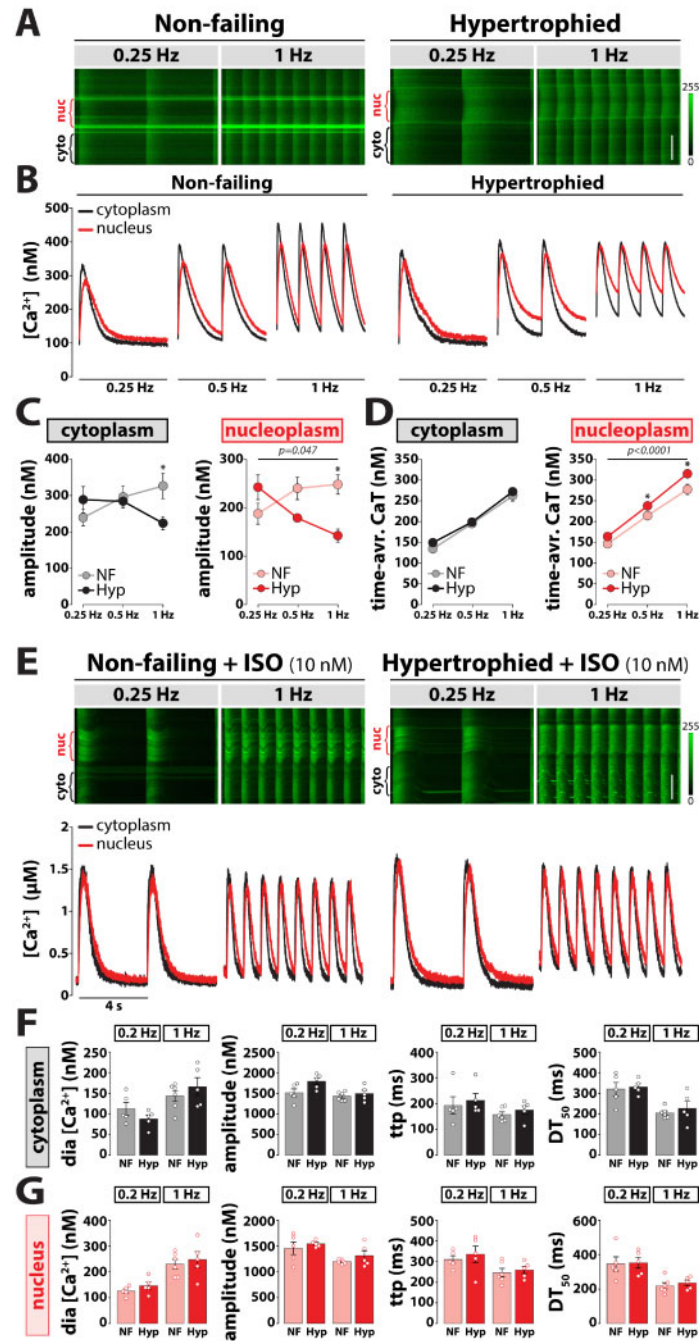


**Figure 7** Impaired subcellular  $\text{Ca}^{2+}$  cycling in response to increased workload in hypertrophied human cardiomyocytes. (A) Original line-scan confocal images of cytoplasmic and nucleoplasmic  $\text{Ca}^{2+}$  transients recorded at 0.25 and 1 Hz stimulation in a ventricular myocyte isolated from non-failing (left) and hypertrophied (right) human hearts. Scale bar, 10  $\mu\text{m}$ . (B) Averaged original recordings of electrically stimulated  $\text{Ca}^{2+}$  transients in the nucleus (red) vs. cytoplasm (black) of ventricular myocytes isolated from non-failing (left) and hypertrophied (right) human hearts in response to gradual increase of stimulation frequency from 0.25 to 1 Hz. (C) Frequency-dependent changes in peak systolic amplitude in electrically stimulated  $\text{Ca}^{2+}$  transient in the cytoplasm (left) vs. nucleus (right) of ventricular myocytes isolated from control and hypertrophied human hearts. (D) Cytoplasmic (left) and nucleoplasmic (right)  $\text{Ca}^{2+}$  load calculated as a time-integral area under  $\text{Ca}^{2+}$  transient-time curve over 1 s in control and hypertrophied cardiomyocytes. (C and D) Data show mean  $\pm$  SEM of  $n = 7$  cells from  $N = 3$  hearts per group,  $P$ -values were calculated using Sidak's *post hoc* test (vs. non-failing at 0.25 Hz), following significant two-way repeated-measures ANOVA. (E) Original line-scan Fluo-4/AM fluorescence recordings (top) of intracellular  $\text{Ca}^{2+}$  transients at baseline and upon acute application of 10 nM isoprenaline (ISO) in a representative control (left) and hypertrophied (right) cardiomyocyte, and corresponding calibrated cytoplasmic (black) and nucleoplasmic (red)  $\text{Ca}^{2+}$  transients (bottom). Mean values of cytoplasmic (F) and nucleoplasmic (G)  $\text{Ca}^{2+}$  transient parameters displaying diastolic (dia)  $[\text{Ca}^{2+}]$ ,  $\text{Ca}^{2+}$  transient amplitude, time-to-peak (ttp), and time from peak  $[\text{Ca}^{2+}]$  to 50% decline ( $\text{DT}_{50}$ ). Data show mean  $\pm$  SEM of  $n = 5$ –6 cells from  $N = 3$  hearts per group. Scale bar, 10  $\mu\text{m}$ . Average data and group comparisons related to Figure 7 are summarized in [Supplementary material online, Table S6](#).

that is regulated via phosphorylation of PLB, and Tnl phosphorylation, which links  $\text{Ca}^{2+}$ -troponin C binding with the activation of crossbridge reactions with the actin filament. Increased phosphorylation of PLB augments the rate and the maximal  $\text{Ca}^{2+}$  uptake by increasing the affinity of SERCA2a for  $\text{Ca}^{2+}$  and its turnover, whereas Tnl Ser-23/24 phosphorylation contributes to  $\text{Ca}^{2+}$  regulation of the myofilament, resulting in decreased  $\text{Ca}^{2+}$ -sensitive force production and accelerated myofilament relaxation.<sup>33,34</sup> Notably, we found that *Atg5*<sup>-/-</sup> mice exposed to isoprenaline showed attenuated positive inotropic responsiveness to  $\beta$ -adrenergic stimulation *in vivo*, which was associated with reduced increase Tnl phosphorylation, but intact PLB phosphorylation. Although previous studies<sup>35–37</sup> that proposed a predominance of the phosphorylation of Tnl over that of PLB to mediate positive inotropy in response to isoprenaline may partly explain the reduced cardiac reserve *in vivo*, reasons for these differences are not entirely clear. At least part of the difference may reflect high pre-existing sympathetic activity during *in situ* assessment (e.g. by catheterization), whereas the use of isolated cardiomyocytes minimizes these influences. In support of this idea, Layland *et al.*<sup>38</sup> demonstrated that reduced phosphorylation of Tnl is linked to contractile dysfunction in conditions similar to those occurring *in vivo* but much less so in the unloaded cardiomyocyte.

ATG5-mediated autophagy failed to directly regulate the subcellular  $\text{Ca}^{2+}$  handling. Along these lines, the properties of the major intracellular  $\text{Ca}^{2+}$  store, SR, including its spatial organization,  $\text{Ca}^{2+}$  content and RyR2-mediated SR  $\text{Ca}^{2+}$  leak, were unchanged in *Atg5*<sup>-/-</sup> cardiomyocytes. In this regard, it is important to mention that mammalian cells lacking ATG5, including *Atg5*<sup>-/-</sup> cardiomyocytes, can still form a fraction of autophagosomes/autolysosomes and perform autophagy-mediated protein degradation via the *Atg5/Atg7*-independent non-canonical pathway.<sup>6</sup> Interestingly, this alternative autophagy process was also proposed to play a predominant role in mediating mitochondrial degradation in the heart during energy deprivation (e.g. ischaemia).<sup>39</sup> Therefore, it is possible that the non-conventional form of autophagy acts as a compensatory mechanism that maintains, at least temporarily, the  $\text{Ca}^{2+}$ -regulatory machinery in young *Atg5*<sup>-/-</sup> mice. However, *Atg5*<sup>-/-</sup> cardiomyocytes displayed accumulated mitochondria aggregates due to impaired mitochondrial clearance,<sup>2,40</sup> which intriguingly coincided with reduced relative mitochondrial mass. This seemingly counterintuitive finding results from decreased individual mitochondrial volume in *Atg5*<sup>-/-</sup> cardiomyocytes and, albeit not measured in our study, can be attributed to balanced mitochondrial degradation vs. biogenesis. In support of this notion, Sun *et al.*<sup>41</sup> recently reported that insufficient autophagy causes reduction in mitochondria content in the heart of a mouse model of lipopolysaccharide-induced sepsis, meanwhile enhanced autophagy in *Becn1-1* transgenic hearts is associated with unexpectedly high mitochondrial abundance.

Apart from rapid  $\text{Ca}^{2+}$  regulation by  $\beta$ -adrenergic signalling, integrative subcellular changes in  $\text{Ca}^{2+}$  levels are critical for cardiac remodelling by modifying  $\text{Ca}^{2+}$ -dependent pathways mediating transcriptional regulation in cardiomyocytes. The selective increase in nucleoplasmic  $\text{Ca}^{2+}$  load at high-pacing frequencies in *Atg5*-deprived mice activated  $\text{Ca}^{2+}$ -dependent signalling involving CaMKII that is known to induce cardiac hypertrophy.<sup>18</sup> Given that persistent overstimulation desensitizes the  $\beta$ -adrenergic signalling pathway, the progression of hypertrophy to heart failure in older *Atg5*<sup>-/-</sup> mice is expected to depend, at least in part, on sustained CaMKII activity. Activated nuclear CaMKII can trigger up-regulation of well-established marker genes linked to pathological hypertrophy, such as *NppB*, *RCAN-1*, *IL-6* receptor, and transforming growth factor (TGF)- $\beta$ 1.<sup>24</sup> Therefore, it is possible that CaMKII regulates  $\text{Ca}^{2+}$ -

mediated gene expression that results from early anomalies in  $\text{Ca}^{2+}$  handling in *Atg5*-deficient mice. Importantly, future studies are warranted to unveil the mechanistic link between autophagy and CaMKII-dependent gene regulation.

Finally, the clinical relevance of our study is presented by the observation that cardiac expression of ATG5 at both transcriptional and protein levels was markedly reduced in hypertrophied and end-stage failing human hearts, while gene and protein expression of ATG5 inversely correlated with the extent of hypertrophy in donor hearts. Importantly, frequency-dependent and isoprenaline-induced changes of subcellular  $\text{Ca}^{2+}$  transients in hypertrophied human cardiomyocytes closely resembled those observed in *Atg5*<sup>-/-</sup> ventricular myocytes. Hence, progressive loss of ATG5 protein and concomitant autophagy impairment parallels the development of hypertrophy and heart failure in humans. Along this line, early impairment of autophagy may cause energy deprivation in stressed myocardium, thereby initiating similar compensatory mechanisms followed by maladaptive events potentially resembling those observed in *Atg5*<sup>-/-</sup> mice. However, although we present a large body of phenomenological evidence that points to a role for ATG5-induced autophagy in  $\text{Ca}^{2+}$  handling in cardiomyocytes, we acknowledge that a direct mechanistic link between impaired autophagy and  $\text{Ca}^{2+}$  cycling abnormalities requires further investigation.

In summary, this study demonstrates reduced mitochondrial abundance and capability to maintain redox balance in *Atg5*-deprived cardiomyocytes under stress. Functional alterations of the cytoplasmic and nucleoplasmic  $\text{Ca}^{2+}$  handling were associated with increased CaMKII activity and concomitant  $\text{Ca}^{2+}$ -mediated transcriptional regulation, and resulted in compromised cardiac functional reserve capacity, which precedes the development of heart failure in both mice and humans.

## Supplementary material

Supplementary material is available at *Cardiovascular Research* online.

## Authors' contributions

S.S. conceptualized the study; S.S. and S.L.-H. designed the study; S.L.-H., S.K., N.D., M.A., J.V., V.H., M.S., M.K., A.N., J.S., K.-M.K., G.F. and J.E. performed the experiments and analysed data; S.L.-H., M.A., C. Mühlfeld, C. Maack, and S.S. interpreted the data; A.Z., D.v.L., P.P.R. and D.S. characterized the patients or provided human cardiac tissue and data; S.L.-H. and S.S. wrote the manuscript. All authors revisited the work critically for important intellectual content and approved the version to be published and agreed to be accountable for all aspects of the work in ensuring that questions related to the accuracy or integrity of any part of the work are appropriately investigated and resolved.

## Acknowledgements

The authors thank Noboru Mizushima (University of Tokyo, Japan) and Kenneth Chien (Harvard University, USA) for their generosity in providing *Atg5*<sup>flox/flox</sup> mice and *MLC2a-Cre*<sup>+</sup> mice, respectively. We are grateful for the excellent support by the animal facility staff of the Institute of Biomedical Research (IBF, Medical University of Graz) for animal wellbeing.

**Conflict of interest:** none declared.

## Funding

This work was supported by the Austrian Science Fund (FWF) (grants P27637-B28 and I3301-MINOTAUR to S.S. and V-530 to S.L.-H.), and BioTechMed-Graz [Young Researcher Groups (YRG) to S.L.-H.]. S.K. was a recipient of the Medical University of Graz scholarship for talented students. M.A. is supported by research grants from the European Society of Cardiology and Austrian Society of Cardiology (Präsidentenstipendium-ÖKG).

## Data availability

The raw data are available from the corresponding author upon reasonable request.

## References

- Abdellatif M, Sedej S, Carmona-Gutierrez D, Madeo F, Kroemer G. Autophagy in cardiovascular aging. *Circ Res* 2018;**123**:803–824.
- Nakai A, Yamaguchi O, Takeda T, Higuchi Y, Hikoso S, Taniike M, Omiya S, Mizote I, Matsumura Y, Asahi M, Nishida K, Hori M, Mizushima N, Otsu K. The role of autophagy in cardiomyocytes in the basal state and in response to hemodynamic stress. *Nat Med* 2007;**13**:619–624.
- Shirakabe A, Ikeda Y, Sciarretta S, Zablocki DK, Sadoshima J. Aging and autophagy in the heart. *Circ Res* 2016;**118**:1563–1576.
- Eisenberg T, Abdellatif M, Schroeder S, Primessnig U, Stekovic S, Pendl T, Harger A, Schipke J, Zimmermann A, Schmidt A, Tong M, Ruckstuhl C, Dambroek C, Gross AS, Herbst V, Magnes C, Trausinger G, Narath S, Meinitzer A, Hu Z, Kirsch A, Eller K, Carmona-Gutierrez D, Büttner S, Pietropaolo F, Knittelfelder O, Schrepfer E, Rockenfeller P, Simonini C, Rahn A, Horsch M, Moreth K, Beckers J, Fuchs H, Gailus-Durner V, Neff F, Janik D, Rathkolb B, Rozman J, de Angelis MH, Moustafa T, Haemmerle G, Mayr M, Willeit P, von Frieling-Salewsky M, Pieske B, Scorrano L, Pieber T, Pechlaner R, Willeit J, Sigrist SJ, Linke WA, Mühlfeld C, Sadoshima J, Dengel J, Kiehl S, Kroemer G, Sedej S, Madeo F. Cardioprotection and lifespan extension by the natural polyamine spermidine. *Nat Med* 2016;**22**:1428–1438.
- Taneike M, Yamaguchi O, Nakai A, Hikoso S, Takeda T, Mizote I, Oka T, Tamai T, Oyabu J, Murakawa T, Nishida K, Shimizu T, Hori M, Komuro I, Takuji Shirasawa TS, Mizushima N, Otsu K. Inhibition of autophagy in the heart induces age-related cardiomyopathy. *Autophagy* 2010;**6**:600–606.
- Nishida Y, Arakawa S, Fujitani K, Yamaguchi H, Mizuta T, Kanaseki T, Komatsu M, Otsu K, Tsujimoto Y, Shimizu S. Discovery of Atg5/Atg7-independent alternative macroautophagy. *Nature* 2009;**461**:654–658.
- Kaushik S, Massey AC, Mizushima N, Cuervo AM. Constitutive activation of chaperone-mediated autophagy in cells with impaired macroautophagy. *Mol Biol Cell* 2008;**19**:2179–2192.
- Levine B, Kroemer G. Biological functions of autophagy genes: a disease perspective. *Cell* 2019;**176**:11–42.
- Ljubojević S, Radulovic S, Leitinger G, Sedej S, Sacherer M, Holzer M, Winkler C, Pritz E, Mittler T, Schmidt A, Sereinigg M, Wakula P, Zissimopoulos S, Bisping E, Post H, Marsche G, Bossuyt J, Bers DM, Kockskamper J, Pieske B. Early remodeling of perinuclear Ca<sup>2+</sup> stores and nucleoplasmic Ca<sup>2+</sup> signaling during the development of hypertrophy and heart failure. *Circulation* 2014;**130**:244–255.
- Sedej S, Schmidt A, Denegri M, Walther S, Matovina M, Arnstein G, Gutsch EM, Windhager I, Ljubojević S, Negri S, Heinzel FR, Bisping E, Vos MA, Napolitano C, Priori SG, Kockskamper J, Pieske B. Subclinical abnormalities in sarcoplasmic reticulum Ca<sup>2+</sup> release promote eccentric myocardial remodeling and pump failure death in response to pressure overload. *J Am Coll Cardiol* 2014;**63**:1569–1579.
- Lehnart SE, Maier LS, Hasenfuss G. Abnormalities of calcium metabolism and myocardial contractility depression in the failing heart. *Heart Fail Rev* 2009;**14**:213–224.
- Wettschreck N, Rutten H, Zywiets A, Gehring D, Wilkie TM, Chen J, Chien KR, Offermanns S. Absence of pressure overload induced myocardial hypertrophy after conditional inactivation of Galpha/Galpa11 in cardiomyocytes. *Nat Med* 2001;**7**:1236–1240.
- Hoit BD, Khoury SF, Kranias EG, Ball N, Walsh RA. In vivo echocardiographic detection of enhanced left ventricular function in gene-targeted mice with phospholamban deficiency. *Circ Res* 1995;**77**:632–637.
- Ayachi M, Niel R, Momken I, Billat VL, Mille-Hamad L. Validation of a ramp running protocol for determination of the true VO<sub>2</sub>max in mice. *Front Physiol* 2016;**7**:372.
- Djalalinac N, Ljubojević-Holzer S, Matzer I, Kolesnik E, Jandl K, Lohberger B, Rainer P, Heinemann A, Sedej S, von Lewinski D, Bisping E. The role of stretch, tachycardia and sodium-calcium exchanger in induction of early cardiac remodeling. *J Cell Mol Med* 2020;**24**:8732–8743.
- Sedej S, Heinzel FR, Walther S, Dybkova N, Wakula P, Groborz J, Gronau P, Maier LS, Vos MA, Lai FA, Napolitano C, Priori SG, Kockskamper J, Pieske B. Na<sup>+</sup>-dependent SR Ca<sup>2+</sup> overload induces arrhythmogenic events in mouse cardiomyocytes with a human CPVT mutation. *Cardiovasc Res* 2010;**87**:50–59.
- Kohlhaas M, Nickel AG, Bergem S, Casadei B, Laufs U, Maack C. Endogenous nitric oxide formation in cardiac myocytes does not control respiration during β-adrenergic stimulation. *J Physiol* 2017;**595**:3781–3798.
- Ljubojević S, Walther S, Asgarzoei M, Sedej S, Pieske B, Kockskamper J. In situ calibration of nucleoplasmic versus cytoplasmic Ca<sup>2+</sup> concentration in adult cardiomyocytes. *Biophys J* 2011;**100**:2356–2366.
- Picht E, Zima AV, Blatter LA, Bers DM. SparkMaster: automated calcium spark analysis with ImageJ. *Am J Physiol Cell Physiol* 2007;**293**:C1073–C1081.
- Kolstad TR, van den Brink J, MacQuaide N, Lunde PK, Frisk M, Aronsen JM, Norden ES, Cataliotti A, Sjaastad I, Sejersted OM, Edwards AG, Lines GT, Louch WE. Ryanodine receptor dispersion disrupts Ca<sup>2+</sup> release in failing cardiac myocytes. *Elife* 2018;**7**:e39427.
- Nickel AG, von Hardenberg A, Hohl M, Löffler JR, Kohlhaas M, Becker J, Reil JC, Kazakov A, Bonnekoh J, Stadelmaier M, Puhl SL, Wagner M, Bogeski I, Cortassa S, Kappl R, Pasioka B, Lafontaine M, Lancaster CR, Blacker TS, Hall AR, Duchon MR, Kästner L, Lipp P, Zeller T, Müller C, Knopp A, Laufs U, Böhm M, Hoth M, Maack C. Reversal of mitochondrial transhydrogenase causes oxidative stress in heart failure. *Cell Metab* 2015;**22**:472–484.
- Haspel J, Shaik RS, Ifedigbo E, Nakahira K, Dolinay T, Englert JA, Choi AM. Characterization of macroautophagic flux in vivo using a leupeptin-based assay. *Autophagy* 2011;**7**:629–642.
- Xie X, Bi HL, Lai S, Zhang YL, Li N, Cao HJ, Han L, Wang HX, Li HH. The immunoproteasome catalytic beta5i subunit regulates cardiac hypertrophy by targeting the autophagy protein ATG5 for degradation. *Sci Adv* 2019;**5**:eaau0495.
- Ljubojević-Holzer S, Herren AW, Djalalinac N, Voglhuber J, Morotti S, Holzer M, Wood BM, Abdellatif M, Matzer I, Sacherer M, Radulovic S, Wallner M, Ivanov M, Wagner S, Sossalla S, von Lewinski D, Pieske B, Brown JH, Sedej S, Bossuyt J, Bers DM. CaMKII $\delta$  drives early adaptive Ca<sup>2+</sup> change and late eccentric cardiac hypertrophy. *Circ Res* 2020;**127**:1159–1178.
- Karczewski P, Bartel S, Krause EG. Differential sensitivity to isoprenaline of troponin I and phospholamban phosphorylation in isolated rat hearts. *Biochem J* 1990;**266**:115–122.
- Briston SJ, Caldwell JL, Horn MA, Clarke JD, Richards MA, Greensmith DJ, Graham HK, Hall MC, Eisner DA, Dibb KM, Trafford AW. Impaired beta-adrenergic responsiveness accentuates dysfunctional excitation-contraction coupling in an ovine model of tachypacing-induced heart failure. *J Physiol* 2011;**589**:1367–1382.
- Bers DM. Cardiac excitation-contraction coupling. *Nature* 2002;**415**:198–205.
- Tripodiadis F, Karayannis G, Giamouzis G, Skoularis J, Louridas G, Butler J. The sympathetic nervous system in heart failure physiology, pathophysiology, and clinical implications. *J Am Coll Cardiol* 2009;**54**:1747–1762.
- Kodama S, Saito K, Tanaka S, Maki M, Yachi Y, Asumi M, Sugawara A, Totsuka K, Shimano H, Ohashi Y, Yamada N, Sone H. Cardiorespiratory fitness as a quantitative predictor of all-cause mortality and cardiovascular events in healthy men and women: a meta-analysis. *JAMA* 2009;**301**:2024–2035.
- Bouchard C, Rankinen T. Individual differences in response to regular physical activity. *Med Sci Sports Exerc* 2001;**33**:S446–S451; discussion S452–S443.
- Campos JC, Queliconi BB, Bozi LHM, Bechara LRG, Dourado PMM, Andres AM, Jannig PR, Gomes KMS, Zambelli VO, Rocha-Resende C, Guatimosim S, Brum PC, Mochly-Rosen D, Gottlieb RA, Kowaltowski AJ, Ferreira JCB. Exercise reestablishes autophagic flux and mitochondrial quality control in heart failure. *Autophagy* 2017;**13**:1304–1317.
- Masiero E, Agatea L, Mammucari C, Blaauw B, Loro E, Komatsu M, Metzger D, Reggiani S, Schiaffino S, Sandri M. Autophagy is required to maintain muscle mass. *Cell Metab* 2009;**10**:507–515.
- Zhang R, Zhao J, Potter JD. Phosphorylation of both serine residues in cardiac troponin I is required to decrease the Ca<sup>2+</sup> affinity of cardiac troponin C. *J Biol Chem* 1995;**270**:30773–30780.
- Ramirez-Correa GA, Cortassa S, Stanley B, Gao WD, Murphy AM. Calcium sensitivity, force frequency relationship and cardiac troponin I: critical role of PKA and PKC phosphorylation sites. *J Mol Cell Cardiol* 2010;**48**:943–953.
- England PJ. Correlation between contraction and phosphorylation of the inhibitory subunit of troponin in perfused rat heart. *FEBS Lett* 1975;**50**:57–60.
- Resink TJ, Gevers W. Dephosphorylation of myofibrillar proteins in actomyosin preparations and in isolated perfused rat hearts after beta-agonist withdrawal. *J Mol Cell Cardiol* 1982;**14**:329–337.
- Rapundalo ST, Solaro RJ, Kranias EG. Inotropic responses to isoproterenol and phosphodiesterase inhibitors in intact guinea pig hearts: comparison of cyclic AMP levels and phosphorylation of sarcoplasmic reticulum and myofibrillar proteins. *Circ Res* 1989;**64**:104–111.

38. Layland J, Grieve DJ, Cave AC, Sparks E, Solaro RJ, Shah AM. Essential role of troponin I in the positive inotropic response to isoprenaline in mouse hearts contracting auxotonically. *J Physiol* 2004;**556**:835–847.
39. Saito T, Nah J, Oka SI, Mukai R, Monden Y, Maejima Y, Ikeda Y, Sciarretta S, Liu T, Li H, Baljinnyam E, Fraidenaich D, Fritzky L, Zhai P, Ichinose S, Isobe M, Hsu CP, Kundu M, Sadoshima J. An alternative mitophagy pathway mediated by Rab9 protects the heart against ischemia. *J Clin Invest* 2019;**129**:802–819.
40. Komatsu M, Waguri S, Ueno T, Iwata J, Murata S, Tanida I, Ezaki J, Mizushima N, Ohsumi Y, Uchiyama Y, Kominami E, Tanaka K, Chiba T. Impairment of starvation-induced and constitutive autophagy in Atg7-deficient mice. *J Cell Biol* 2005;**169**:425–434.
41. Sun Y, Yao X, Zhang QJ, Zhu M, Liu ZP, Ci B, Xie Y, Carlson D, Rothermel BA, Sun Y, Levine B, Hill JA, Wolf SE, Minei JP, Zang QS. Beclin-1-dependent autophagy protects the heart during sepsis. *Circulation* 2018;**138**:2247–2262.

### Translational perspective

Autophagy is a cytoprotective process ensuring homeostasis of the heart. Here, we report that maladaptive hypertrophy and heart failure associate with reduced expression of autophagy-related protein 5 (ATG5) in humans. In mice, ATG5-dependent autophagy disrupts subcellular  $\text{Ca}^{2+}$  homeostasis and  $\text{Ca}^{2+}$ -mediated transcriptional regulation, coinciding with impaired mitochondrial redox balance, especially during stress and increased cardiac demand. These effects translate into reduced cardiac functional reserve capacity and the development of premature heart failure. Hence, re-instating autophagy at early stages of cardiac remodelling may protect from heart failure through preserving mitochondrial abundance and nuclear  $\text{Ca}^{2+}$  homeostasis.